



**HAL**  
open science

## Modelling slit tape buckling during automated prepreg manufacturing: A local approach

Alexis Beakou, Miguel Cano, Jean-Benoit Le Cam, Vincent Verney

► **To cite this version:**

Alexis Beakou, Miguel Cano, Jean-Benoit Le Cam, Vincent Verney. Modelling slit tape buckling during automated prepreg manufacturing: A local approach. *Composite Structures*, 2011, 93, pp.2628-2635. 10.1016/j.compstruct.2011.04.030 . hal-01131580

**HAL Id: hal-01131580**

**<https://hal.science/hal-01131580>**

Submitted on 19 Apr 2018

**HAL** is a multi-disciplinary open access archive for the deposit and dissemination of scientific research documents, whether they are published or not. The documents may come from teaching and research institutions in France or abroad, or from public or private research centers.

L'archive ouverte pluridisciplinaire **HAL**, est destinée au dépôt et à la diffusion de documents scientifiques de niveau recherche, publiés ou non, émanant des établissements d'enseignement et de recherche français ou étrangers, des laboratoires publics ou privés.

# Modelling slit tape buckling during automated prepreg manufacturing: A local approach

A. Beakou <sup>a,\*</sup>, M. Cano <sup>a</sup>, J.-B. Le Cam <sup>a</sup>, V. Verney <sup>b,c</sup>

<sup>a</sup> Clermont Université, IFMA, Laboratoire de Mécanique et Ingénieries, BP 10448, F-63000 Clermont-Ferrand, France

<sup>b</sup> Clermont Université, UBP, Laboratoire de Photochimie Moléculaire et Macromoléculaire, BP 10448, F-63000 Clermont-Ferrand, France

<sup>c</sup> CNRS, UMR6505, LPMM, F-63173 Aubière, France

This paper investigates the local buckling of slit tape in the Automated Fibre Placement process for a circular fibre path using an analytical approach that accounts for prepreg tack and stress distribution. Curing effects are not considered in this study. The main objective is to define the critical buckling load and therefore the minimal steering radius for which no tow wrinkling occurs. Simulations are performed for the buckling of the first ply, using a tack parameter governing the interaction between tool and material. A sensitivity analysis of the most relevant parameters of the model is performed. Numerical results show that lower values of the steering radius are obtained for lower tow width values and higher prepreg tack values. Experimental investigations show that the estimation of wrinkling occurrence in steered fibres could be improved by taking into account certain additional parameters, such as lay-down rate, temperature and the dynamic behaviour of the resin.

## 1. Introduction

Composite materials have been used for 30 years to replace various aluminium alloys in modern aircraft, resulting in a significant positive effect on performance, weight, design and energy consumption. Carbon fibres are mainly used to manufacture airframe structures because of their high stiffness and strength. Preimpregnated plies, or prepregs, are sheets of unidirectional fibres coated with a thermoplastic or partially cured thermoset resin. Prepreg generally performs better structurally than the corresponding dry fabric/resin impregnation method, thanks to better manufacturing controls [1].

Earlier composite airframe structures were manufactured by hand lay-up. The hand lay-up technique is a time-consuming process, especially for large components. It is a labour-intensive process in which the quality of the parts is based on the skills of the operators. The chemical emission of this open process is high, which may lead to safety and environmental issues. The first automated manufacturing technique developed to enhance product quality and increase productivity is the so-called Automated Tape Laying (ATL) method. ATL uses large wide tapes (150 mm or 300 mm width) which are suitable for producing parts with flat or single large curvature radius surfaces (i.e. keel beam, cross beams, center wing box). For complex parts with double curvature

radius surfaces, steering of prepreg tapes might be required to maintain the desired fibre orientation. Then an innovative technique, Automated Fibre Placement (AFP), was developed, combining the advantages of tape laying and filament winding with advanced computer control and software in order to produce economically high-quality contoured structures [2–4]. AFP, also called ATP for Automated Tow Placement, consists in laying down simultaneously a large number (up to 32) of tows of 3.175–12.7 mm width (Fig. 1a) to manufacture laminates with a continuously varying fibre orientation angle. AFP is a promising technology that enables designers to enhance the performance of composite structures. Lopes et al. demonstrate the advantages of variable-stiffness over straight-fibre laminates in terms of compressive buckling and first-ply failure [5]. In Ref. [6], Blom et al. use different path definitions for variable-stiffness shells to optimize conical shells for the maximum fundamental frequency. The authors show that it is necessary to take the manufacturing constraints into account in the design phase of composite structures.

However, automated manufacturing techniques have their limitations. If the turning radius of the placement head is too small, the fibres tend to wrinkle out-of-plane (Fig. 1c), which could lead to defects that degrade the structural load-carrying capabilities of the cured laminate. Adam and Hyer showed a decrease in strength as great as 36% [7]. These fabrication-induced defects are called “ply waviness” and belong to the group of so-called “marcel defects” referring to Marcel Grateau’s hair style. Fig. 1d shows actual marcel defects in a composite part [8].

\* Corresponding author.

E-mail address: Alexis.Beakou@ifma.fr (A. Beakou).

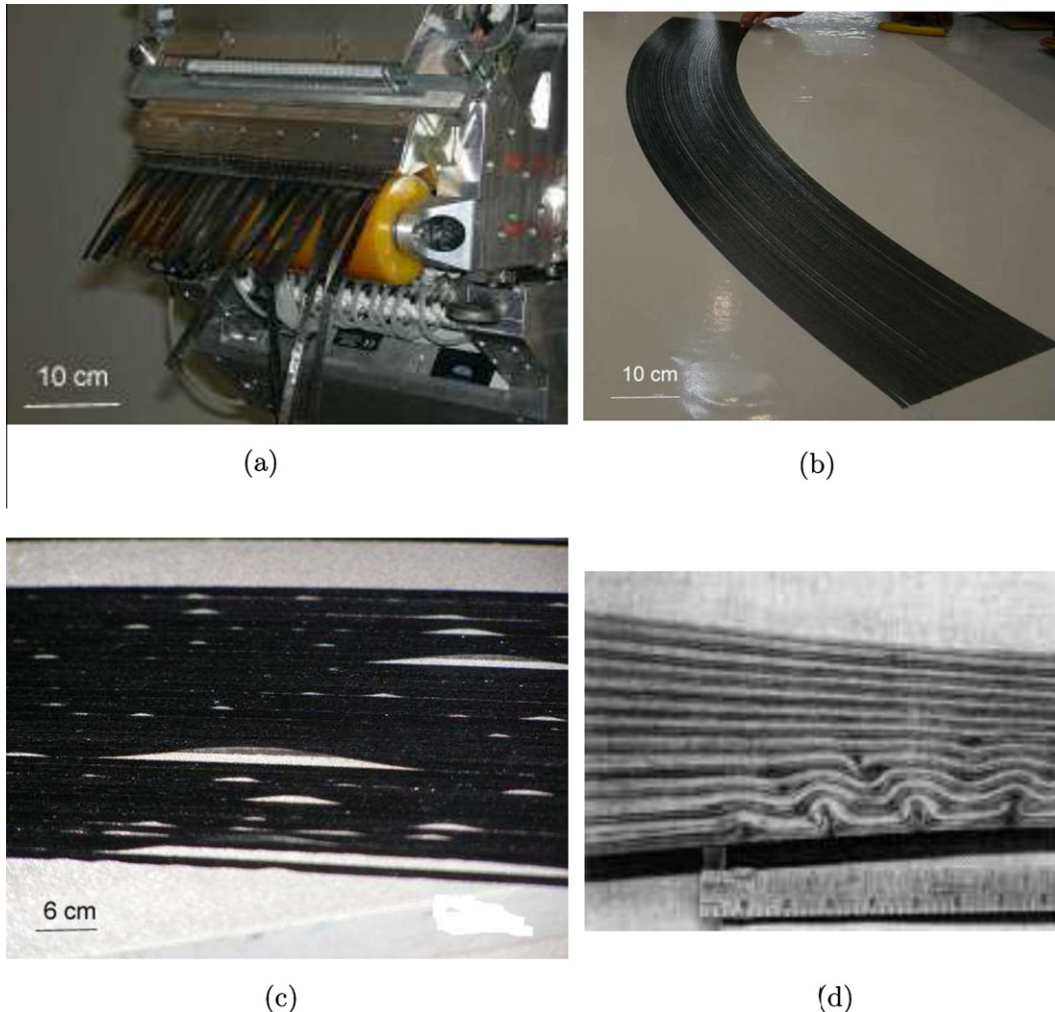


**Fig. 1.** Automated Fibre Placement and ply waviness. (a) AFP placement head with 32 fibres of 6.35 mm width. (b) Streered fibres in the first ply. (c) Local buckling of streered fibres. (d) Ply waviness in a compsite part [8].

Most studies focus on the effects that ply waviness have on cured composite structural properties; stiffness, static strength and residual strength after low-cycle fatigue loading [7–12]. The ply waviness formation mechanism has not given rise to many studies and remains unclear, since these defects occur at different steps in the manufacturing process. Aircraft companies have developed technological expertise to avoid ply waviness formation. Studying the optimization of fibre paths for composite design, Nagendra et al. suggest a minimum turning radius of the placement head of 635 mm to avoid local fibre buckling [13]. However, it is still necessary to conduct a thorough study to establish the relationship between the process parameters and waviness formation. Ng and Vizzini used a fibre optic based process measurement technique to determine the time and compaction pressure at which waviness formation occurs [14]. Zhou used high-powered ultrasonics to establish the critical material and process parameters that affect waviness formation during the curing step in compression molding [15]. The author found that a higher mold temperature and a lower pressure rate lead to reduced waviness.

To summarize, waviness formation is studied in the literature using mostly experimental or semi-empirical approaches. To our knowledge, there is no paper using analytical modelling to determine the conditions of tow waviness occurrence in the AFP process.

Tow wrinkling formation is a local phenomenon as it arises from tool/prepreg interaction during material lay-down. It results

from the buckling of a tow element compressed between the tool and the placement head in rotation. Compaction force strongly influences the level of adhesion of the prepreg, also called prepreg tack [16,17]. The latter expression will be used in this paper. To efficiently take into account the interaction between tool and material, an element of the steered tow resting on elastic foundations must be considered. Seide was amongst the earliest researchers to study the buckling of plates resting on elastic foundations [18]. Most practical applications are encountered in civil engineering and are based on the local buckling of composite steel-concrete using one half wave [19,20]. An extensive review of the research on composite plate buckling behaviour is presented in Ref. [21]. In aeronautics and marine engineering, analytical tools based on explicit closed-form solutions for both isotropic [22] and orthotropic [23] materials are used to estimate buckling load and post-buckling behaviour in the preliminary design phase of stiffened panels.

In this paper, we propose to investigate the formation of tow wrinkling in the AFP process for a circular fibre path using an analytical approach that accounts for prepreg tack and stress distribution. Our research is limited to the first ply (Fig. 1b) and curing effects are not studied. The main objective is to define the critical buckling load and therefore the minimal radius of curvature for which no tow wrinkling occurs. Moreover, a sensitivity analysis of the most relevant parameters is performed and experimental investigations are undertaken to validate the model. The paper is

divided into four parts. In the first part, we present the governing equation for local buckling of anisotropic plates resting on elastic foundations. The second part is dedicated to the identification of model parameters: geometrical parameters, mechanical properties of materials constituting the prepreg and the interface parameters between the prepreg and the tool. Stress distribution will be taken into account using a load parameter  $\alpha$ . In the third part, we perform numerical simulations to evaluate critical buckling loads and analyse the influence of the most relevant parameters. Finally, in the fourth and last part, estimated and measured values are compared and concluding remarks are made.

## 2. Modelling approach

In the context of the local phenomenon studied, let us consider a thin anisotropic plate made of carbon prepreg of length  $a$ , width  $b/2$ , thickness  $h$ , resting on an elastic foundation of normal stiffness  $k_N$  which is a measure for the adhesion of the tow to the underlying surface. We take the coordinate system of the thickness direction of the plate, such that the reference plane is placed in the central plane of the plate (Fig. 2). The material used is an M21/35%/268/T700GC provided by Hexcel Composites, Dagneux, France. The material is transversely isotropic in the global coordinate system. The dynamic modulus of uncured M21 resin is measured by DMA. Identification of the normal interaction stiffness  $k_N$  will be described in Section 3.

### 2.1. Assumptions

- According to the processing conditions and testing observations, the edge of the plate at the inner radius of curvature should be free in order to allow wrinkling out of plane. We assume that the three others edges are simply supported to allow for an analytical solution. It is worth noting that when buckling occurs, the tow waviness is first compressed by the roller and then recovers after the passage of the placement head.
- The plate is subjected to combined in-plane bending and tension in the slit tape transported by its guidance systems from the magazine creel to the placement head. Then the position of the neutral axis of the resulting in-plane stress distribution varies and is controlled in this study by a load parameter  $\alpha$ .
- Given the plate dimensions, classic laminated plate theory will be applied with the Kirchhoff–Love hypothesis (normals to the mid-plane before steering remain normal to the deformed mid-plane) and von Kármán approximations (in-plane effects are infinitesimal compared to the effect of the deflection  $w$ ) [22].

### 2.2. Variational formulation and the Ritz method

Instead of FE analysis, the Ritz method is used in this section to evaluate the critical buckling load because closed-form solutions

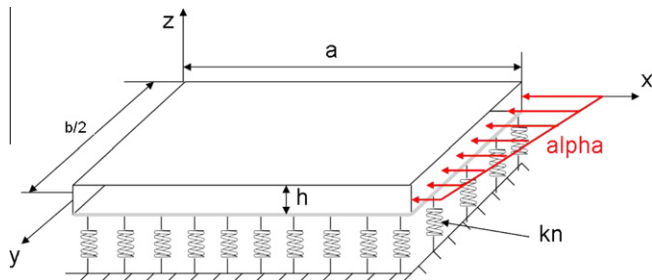


Fig. 2. Anisotropic plate on one-parameter elastic foundation.

can be derived, giving insight into the parameters influencing the manufacturing process. This method has the added advantage of high accuracy and computational efficiency in the study of vibration and buckling of orthotropic plates when efficient admissible functions are used [24,25].

Assuming the Kirchhoff–Love hypothesis and von Kármán approximations and denoting  $w$  the deflection of the plate, the Ritz method requires that the functional  $\Pi(w)$  be minimized.

$$\Pi(w) = U(w) + V(w) - T(w) \quad (1)$$

$U(w)$ ,  $V(w)$  and  $T(w)$  are the elastic strain energy of the plate, the potential energy of the foundation and the potential energy of the in-plane compression stress distribution, respectively.

$$U(w) = \frac{1}{2} \int_0^a \int_0^{b/2} \left[ D_{11} \left( \frac{\partial^2 w}{\partial x^2} \right)^2 + D_{22} \left( \frac{\partial^2 w}{\partial y^2} \right)^2 + 2D_{12} \frac{\partial^2 w}{\partial x^2} \frac{\partial^2 w}{\partial y^2} + 4D_{66} \left( \frac{\partial^2 w}{\partial x \partial y} \right)^2 \right] dx dy$$

$$V(w) = \frac{1}{2} \int_0^a \int_0^{b/2} k_N \cdot w^2 dx dy$$

$$T(w) = \frac{1}{2} \int_0^a \int_0^{b/2} \bar{N}_{xx} \left( \frac{\partial w}{\partial x} \right)^2 dx dy$$

$$D_{ij} = \int_{-\frac{h}{2}}^{\frac{h}{2}} C_{ij} z^2 dz$$

are the bending rigidity and

$$C_{11} = \frac{E_L}{1 - \nu_{LT}\nu_{TL}}; \quad C_{12} = \frac{\nu_{LT}E_T}{1 - \nu_{LT}\nu_{TL}}$$

$$C_{22} = \frac{E_T}{1 - \nu_{LT}\nu_{TL}}; \quad C_{66} = 2G_{LT}$$

$E_L$ ,  $E_T$ ,  $\nu_{LT}$  and  $G_{LT}$  are the elastic properties of the prepreg and they are calculated from the volume fraction of the constituents and fibre and matrix properties using homogenization techniques.

Commonly, the following deflection shape is used when plate buckling problems are solved by the Ritz method.

$$w(x, y) = \sum_{m=1}^{\infty} \sum_{n=1}^{\infty} a_{mn} \sin\left(\frac{m\pi x}{a}\right) \sin\left(\frac{2n\pi y}{b}\right) \quad (2)$$

where  $a_{mn}$  are free constants.

This function satisfies the boundary conditions for a plate with four simply supported edges. In this study, we have one edge free, and the three others are assumed simply supported, so we perform a mirror symmetry of the plate around the edge  $y = b/2$  (Fig. 3). Therefore, calculations will be performed on a plate of length  $a$  and width  $b$ , simply supported on all four edges, and Eq. (2) is rewritten as:

$$w(x, y) = \sum_{m=1}^{\infty} \sum_{n=1}^{\infty} a_{mn} \sin\left(\frac{m\pi x}{a}\right) \sin\left(\frac{n\pi y}{b}\right) \quad (3)$$

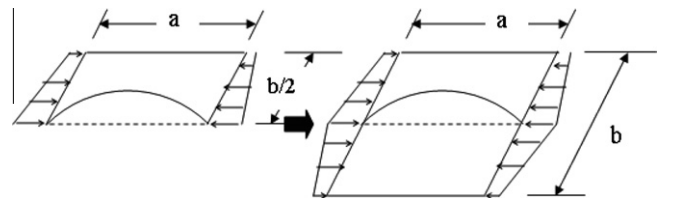


Fig. 3. Mirror symmetry of the plate.

Then the in-plane compressive load can be expressed as:

$$\bar{N}_{xx}(y) = \begin{cases} N_0 \left[ (1 - \alpha) + \frac{2xy}{b} \right] & \text{if } 0 \leq y \leq \frac{b}{2} \\ N_0 \left[ (1 + \alpha) - \frac{2xy}{b} \right] & \text{if } \frac{b}{2} \leq y \leq b \end{cases} \quad (4)$$

The distribution of applied in-plane stress  $\bar{N}_{xx}(y)$  is controlled by the load parameter  $\alpha$ .  $N_0$  is the maximum stress value. Fig. 4 represents the distribution of  $\bar{N}_{xx}(y)$  for  $\alpha = 0$ ,  $\alpha = 1$  and  $\alpha = 2$ . The fibre placement system is designed to minimize the tension in the tows to enable the placement of fibres on concave surfaces. Steering adds a bending component, and therefore  $\alpha$  is expected to have a value between 1 and 2.

Using Eqs. (3) and (4), Eq. (1) is rewritten as:

$$\Pi = \frac{ab}{8} \sum_{m=1}^{\infty} \sum_{n=1}^{\infty} \left[ a_{mn}^2 (E_{mn} + H_{mn}) - N_0 \left( a_{mn}^2 F_{mn} + \sum_{q=1}^{\infty} a_{mn} a_{mq} G_{mnq} \right) \right] \quad (5)$$

with

$$\begin{aligned} E_{mn} &= \left[ D_{11} \left( \frac{m\pi}{a} \right)^4 + D_{22} \left( \frac{n\pi}{b} \right)^4 + (2D_{12} + 4D_{66}) \left( \frac{m\pi}{a} \right)^2 \left( \frac{n\pi}{b} \right)^2 \right] \\ H_{mn} &= k_N \\ F_{mn} &= \left( \frac{m\pi}{a} \right)^2 \left\{ 1 + \alpha \left( \frac{1}{n^2 \pi^2} [1 - (-1)^n] - \frac{1}{2} \right) \right\} \\ G_{mnq} &= \frac{8\alpha}{\pi^2} \left( \frac{m\pi}{a} \right)^2 \left\{ \frac{-1^{\frac{n-q}{2}} - 1}{(n-q)^2} - \frac{-1^{\frac{n+q}{2}} - 1}{(n+q)^2} \right\} \end{aligned} \quad (6)$$

and  $n \neq q$  and  $n \pm q$  even.

Equilibrium conditions require that the first variations of functional  $\Pi$ , which represents the total potential energy of the plate, are set at zero, that is to say

$$\frac{\partial \Pi}{\partial a_{mn}} = 0 \quad \text{for all } (m, n) \in (\mathbb{N}^{*2})$$

This condition leads to

$$2a_{mn}(E_{mn} + H_{mn}) - N_0 \left( 2a_{mn}F_{mn} + \sum_{q=1}^{\infty} a_{mq}G_{mnq} \right) = 0 \quad \text{for all } (m, n) \in (\mathbb{N}^{*2}) \quad (7)$$

$n \neq q$  and  $n \pm q$  even.

In this study, only the first buckling mode is required, so  $m = 1$ . Next, we can expand Eq. (7) for  $1 \leq n \leq 2k$  to obtain

$$\begin{pmatrix} 2(E_{11} + H_{11}) & 0 & 0 & \cdots & 0 \\ 0 & 2(E_{12} + H_{12}) & 0 & \cdots & 0 \\ 0 & 0 & 2(E_{13} + H_{13}) & \cdots & 0 \\ \cdots & \cdots & \cdots & \cdots & \cdots \\ 0 & 0 & 0 & \cdots & 2(E_{1(2k)} + H_{1(2k)}) \end{pmatrix} \begin{pmatrix} a_{11} \\ a_{12} \\ a_{13} \\ \vdots \\ a_{1(2k)} \end{pmatrix} = \begin{pmatrix} 0 \\ 0 \\ 0 \\ \vdots \\ 0 \end{pmatrix} - N_0 \begin{pmatrix} 2F_{11} & 0 & G_{113} & \cdots & 0 \\ 0 & 2F_{12} & 0 & \cdots & G_{12(2k)} \\ G_{131} & 0 & 2F_{13} & \cdots & 0 \\ \vdots & \vdots & \vdots & \vdots & \vdots \\ 0 & G_{1(2k)2} & 0 & \cdots & 2F_{1(2k)} \end{pmatrix} \begin{pmatrix} a_{11} \\ a_{12} \\ a_{13} \\ \vdots \\ a_{1(2k)} \end{pmatrix} = \begin{pmatrix} 0 \\ 0 \\ 0 \\ \vdots \\ 0 \end{pmatrix} \quad (8)$$

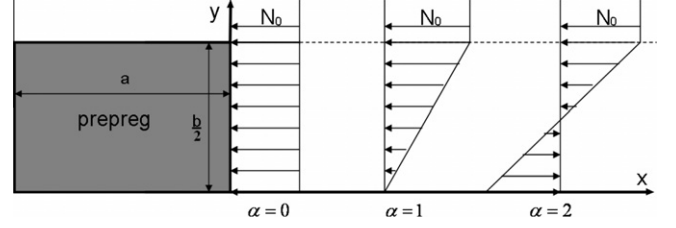


Fig. 4. Distribution of applied in-plane stress for  $\alpha = 0$ ,  $\alpha = 1$  and  $\alpha = 2$ ;  $\alpha$  is expected to have a value between 1 and 2.

Eq. (8) can be rewritten concisely in the form:

$$([K] - N_0[S]) \begin{Bmatrix} a_{11} \\ \vdots \\ a_{1(2k)} \end{Bmatrix} = \begin{Bmatrix} 0 \\ \vdots \\ 0 \end{Bmatrix} \quad (9)$$

where  $[K]$  is the stiffness of the plate and the elastic foundation.  $[S]$  represents the stress-stiffness matrix. Then Eq. (8) appears as a generalized eigenvalue problem. Only the lowest eigenvalue,  $N_{0cr}$ , which represents the critical buckling load, is of interest to our work. The accuracy of the critical load depends on the size of the matrices. A convergence study, carried out in our research group, shows that  $(3 \times 3)$  is the optimal matrix size.

### 2.3. Expression of the critical steering radius of the fibre

Once  $N_{0cr}$  has been calculated, the corresponding steering radius is deduced by using the relation between the bending moment and the curvature of the tow. For this purpose, the tow is treated as a beam of width  $h$  and height  $b/2$ . The adhesion between the prepreg and the tool is neglected.

Using Eq. (4), the distribution of the normal stress  $\sigma_{xx}$  is written in the form:

$$\sigma_{xx} = \frac{\bar{N}_{xx}(y)}{h} = \frac{N_{0cr}}{h} \left[ (1 - \alpha) + \frac{2xy}{b} \right], \quad 0 \leq y \leq \frac{b}{2} \quad (10)$$

Denoting  $\sigma_{xx}^o = \sigma_{xx}(\frac{b}{4}) = \frac{N_{0cr}}{h} (1 - \frac{\alpha}{2})$ , the normal stress  $\sigma_{xx}$  is rewritten as:  $\sigma_{xx} = \sigma_{xx}^b + \sigma_{xx}^o$  where  $\sigma_{xx}^b = \frac{\alpha N_{0cr}}{2h} [-1 + \frac{4y}{b}]$  is the normal stress resulting from pure bending.

The relation between the bending moment  $M_z$  and the curvature  $\frac{1}{r}$  is expressed as [26]:

$$\frac{1}{r} = \frac{d^2 y}{dx^2} \frac{M_z}{E_L I} \quad (11)$$

where  $E_L$  is the longitudinal Young's modulus of the tow and  $I = \frac{hb^3}{96}$  the second moment of area of the tow cross section.

The bending moment  $M_z$  is expressed as:

$$M_z = 2 \int_0^{b/4} h \sigma_{xx}^b \left( \frac{b}{4} - y \right) dy = 2 \int_{b/4}^{b/2} h \sigma_{xx}^b \left( y - \frac{b}{4} \right) dy = \frac{\alpha N_{0cr} b^2}{48} \quad (12)$$

Finally, using Eqs. (11) and (12), the critical radius of curvature of the tow is expressed as:

$$r = \frac{E_L b h}{2 \alpha N_{0cr}} \quad (13)$$

In the following section, we will identify the various parameters involved in the problem in order to carry out numerical simulations.

### 3. Identification of model parameters

#### 3.1. Geometrical parameters

- The width  $b/2$  and the thickness  $h$  of the plate are measured during the slit tape acceptance tests; the mean values obtained are  $b/2 = 6.35$  mm and  $h = 0.26$  mm. Tow width is one of the more important parameters that aircraft manufacturers can vary. Therefore, sensitivity analysis will be investigated for a tow width  $b/2$  varying between 3.18 mm to 12.7 mm ( $1/8$ – $1/2$ ”). The length  $a$  must be small enough for the rectangular approximation of the plate to be acceptable; let  $a_{max} = 6.35$  mm.

#### 3.2. Elastic properties of the prepreg

Unidirectional prepregs are transversally isotropic. The theory of transversally isotropic thin plates requires only four elastic constants, namely  $E_L$ ,  $E_T$ ,  $\nu_{LT}$  and  $G_{LT}$ . In this paper, these elastic properties are calculated from the volume fraction of the constituents and fibre and matrix properties using Puck's formulas [27].

$$E_L = \phi_f E_f + (1 - \phi_f) E_m$$

$$E_T = \frac{E_m}{1 - \nu_m^2} \left[ \frac{1 + 0.85\phi_f^2}{(1 - \phi_f)^{1.25} + \frac{E_m}{E_f} \frac{\phi_f}{1 - \nu_m^2}} \right]$$

$$G_{LT} = G_m \left[ \frac{1 + 0.6\phi_f^{0.5}}{(1 - \phi_f)^{1.25} + \phi_f \frac{G_m}{G_f}} \right]$$

$$\nu_{LT} = \phi_f \nu_f + (1 - \phi_f) \nu_m$$

The T700 GC carbon fibres reinforcing the prepreg were manufactured by Toray. Young's modulus,  $E_f = 230$  GPa, was taken from Ref. [28]. The Poisson ratio of T700 GC was not available in the product data given by the manufacturer, so the value  $\nu_f = 0.20$  of carbon fibre from Ref. [29] was used. Identification of the Young's modulus of the uncured epoxy resin used DMA tests performed at 30 °C. The modulus calculated over a large range of frequencies is about  $E_m = 0.053$  MPa, which is very low compared to the Young's modulus of carbon fibre. O'Brien et al. studied the cure-dependent viscoelastic Poisson's ratio of two commercial epoxy resins using Moiré interferometry [30]. They found that this property evolves from an elastic value of about 0.4 to a rubbery plateau value of 0.49 at long time values. As long time effects are not taken into account in our model, we took  $\nu_m = 0.4$  for the uncured M21 resin. Finally a value of 0.569 for the nominal volume fibre fraction was taken from Ref. [31]. Computed engineering properties of the tow using Puck's formulas are reported in Table 1.

#### 3.3. Identification of the properties of the foundation

The tack of a material is commonly defined as the sensation one experiences when removing one's finger from any sticky material. In the community of composite materials, tack is the property required to produce a sufficient bond between prepreg plies (or tool and prepreg ply), but not too high, so that a misplaced prepreg ply can be relocated [16]. Peel tests could be used to measure tack, but the extraction of tack parameters is hard to perform. The most appropriate tack measurement seems to come from the work deal-

**Table 1**  
Engineering properties of the tow.

$E_L$ (GPa)	$E_T$ (MPa)	$G_{LT}$ (MPa)	$\nu_{LT}$
131	0.231	0.079	0.286

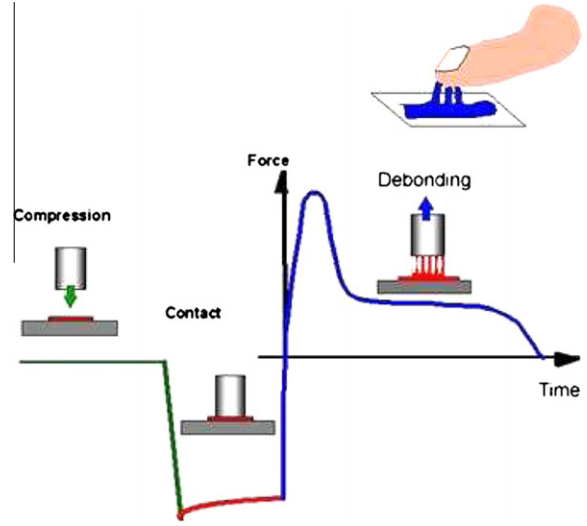
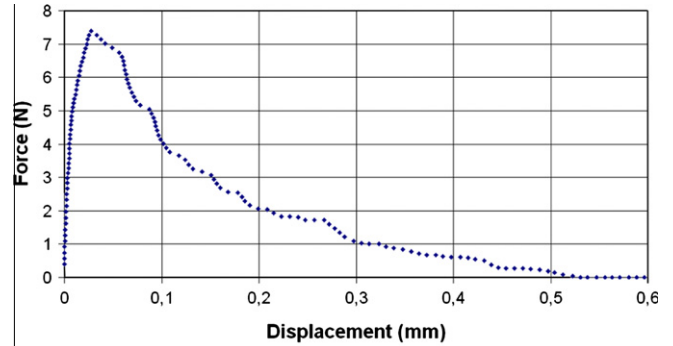


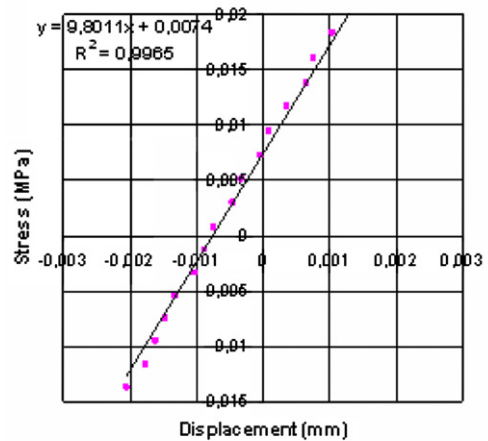
Fig. 5. Schematic of a probe tack test [32].

ing with pressure sensitive adhesives [32]. It is called the *probe tack test* and consists of a probe that comes into contact with the material to be characterized; it is then removed and the separation force and energy are measured (Fig. 5).

In the present study, the normal interface stiffness  $k_N$  is measured using a suitable measurement apparatus recently developed



(a) Force plotted against probe displacement in the removal phase.



(b) Calculation of  $k_N$ .

Fig. 6. Identification of the normal stiffness  $k_N$ .

by our research group [17]. For this purpose, a 1 kN Instron 5543 universal testing machine (Norwood, MA, USA) was used with software which allowed us to define the specific cycle corresponding to the probe tack test.

The test procedure used for tack measurement aims to apply similar loading and environmental conditions as during fibre placement. This procedure is shortly described hereafter:

- Prepreg strip samples were put in a climatic chamber for 30 min at a controlled temperature, here 30 °C.
- Before each run, the contact surface of the probe and the support were cleaned with acetone.
- Contact time, contact force and the debonding rate were set at 10 s, 15 N and 5 mm min<sup>-1</sup>, respectively.
- The temperature of the probe was set at 30 °C via a regulator.
- Once the temperature of the probe reached the set point and was equilibrated, the sample was removed from the climatic chamber and positioned on the support. It should be noted that the side of the prepreg protected by a release paper, i.e. the tackiest side, was applied without pressure on the lower grip.
- The value given by the load cell was reset and the test started.
- Time, force and crosshead displacement were then recorded.

Fig. 6 shows the force–displacement curve during the removal phase when the probe used for the test has a diameter of 10 mm.

The stiffness in the normal direction is given by the equation of the curve in the outlined zone. Thus the normal stiffness  $k_N$  is taken as  $9.8 \times 10^9$  N/m<sup>3</sup>.

#### 4. Numerical results and comments

In this section, the influence of the most relevant parameters, namely  $a$ ,  $b$ ,  $k_N$  and  $\alpha$ , on the minimal steering radius will be studied.

##### 4.1. Influence of the length “a” of the plate

Fig. 7 represents the minimum steering radius of the tow plotted against the length “a” of the plate for  $\alpha = 1$ ,  $b/2 = 6.35$  mm and for various values of  $k_N$ . We can see the influence of the interface stiffness on the radius. For  $a = 4$  mm, the minimum steering radius increases from 865 mm to 950 mm when  $k_N$  decreases from  $10 \times 10^9$  N/m<sup>3</sup> to 0 N/m<sup>3</sup>. This explains why the tack of prepreg material is currently a research area of importance. The second point of information resulting from Fig. 7 is that for lower values of “a”, the influence of the tack decreases and a much lower steering radius could be performed without local buckling. The value suggested by Nagendra et al. [13] is obtained

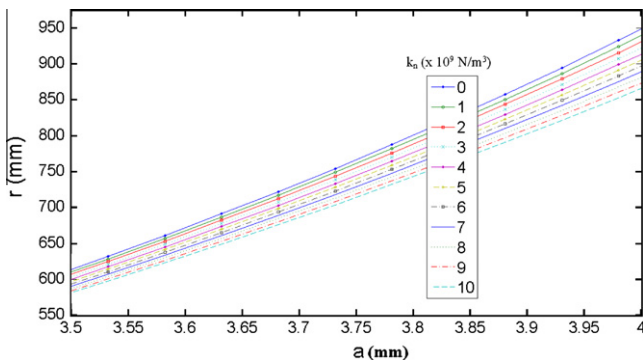


Fig. 7. Minimum steering radius of the tow plotted against length “a” for  $\alpha = 1$ ,  $b/2 = 6.35$  mm and for various values of  $k_N$ .

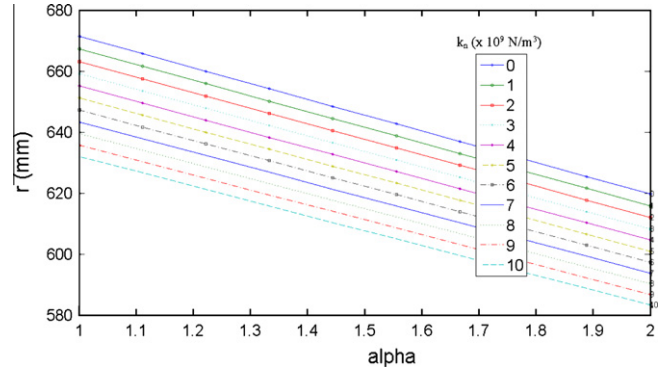


Fig. 8. Minimum steering radius of the tow plotted against  $\alpha$  for  $a = 3.6$  mm,  $b/2 = 6.35$  mm and for various values of  $k_N$ .

for approximately  $a = 3.6$  mm, which belongs to the range of values investigated.

##### 4.2. Influence of the stress distribution factor $\alpha$

Fig. 8 represents the minimum steering radius of the tow plotted against the stress distribution factor  $\alpha$  for  $a = 3.6$  mm and for various values of  $k_N$ . The introduction of a stress factor  $\alpha$  aims to account for unknown additional stresses to the bending effect, induced by various technological devices involved in the guidance of the slit tape. Fig. 8 shows that the pure bending case ( $\alpha = 2$ ) gives the lowest values of the minimum steering radius. However, in pure bending the outer radius of the tow will be stretched. This could produce lateral compressive stresses leading to a transverse buckling phenomenon [33] (not studied here) with the likelihood of lift at the outer edge. Here again, the tack of the prepreg modeled by the interface stiffness  $k_N$  strongly influences the minimum steering radius without local buckling.

##### 4.3. Influence of the tow width $b/2$

Fig. 9 represents the minimum steering radius of the tow plotted against  $b$ , the double width of the plate, for  $\alpha = 1$ ,  $a = 3.6$  mm and for various values of  $k_N$ . We can see that lower values of steering radii without buckling are obtained for a narrow tow. For example, the minimum steering radius decreases from 1400 mm to 650 mm when the tow width  $b/2$  decreases from 12.7 mm to 6.35 mm. Then, the tow width appears as one of the more important parameters that aircraft manufacturers can vary to produce complex parts.

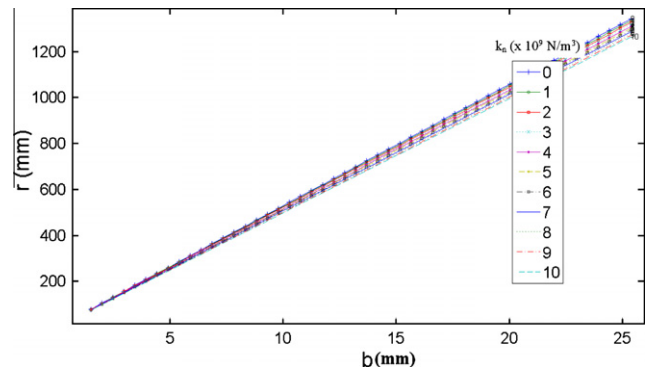


Fig. 9. Minimum steering radius of the tow plotted against  $b$  for  $a = 3.6$  mm,  $\alpha = 1$  and for various values of  $k_N$ .

## 5. Experimental validation

Steering tow tests were performed on the FPV-ATLAS machine at Forest Liné, Capdenac, France. The material used was an M21/35%/268/T700GC provided by Hexcel Composites, Dagneux, France. It was taken out of the freezer 48 h before testing. The temperature in the testing room was 21° and the relative humidity was 40%. An infrared lamp was used to raise the temperature of the material to approximately 35° just before application of the compaction force. The occurrence of waviness was checked immediately after fibre placement. It was not possible to evaluate in situ parameters such as prepreg tack, so qualitative results will be given hereafter.

### 5.1. Influence of compaction force

The prepreg was placed on a steel table without any preparation. The roller was made of rubber. The lay-down rate was 12 m/min, the heating power was 1500 W and the compaction force varied from 1000 to 3000 N. The results showed that, for a given steering radius, lower compaction forces led to placement without tow wrinkling. Typically, for a steering radius of 3.5 m, tow wrinkling was observed on the slit tape for a compaction effort of 3000 N, while with a compaction force of 2000 N none was observed. However, it was observed that below a compaction force of 1500 N, prepreg tack was not high enough to stick the material to the steel table, which led to a general detachment of the slit tape. The correlation between prepreg tack and compaction force should be established and taken into account in the model.

### 5.2. Influence of the prepreg tack

The previous roller was used again and the lay-down rate and heating power were unchanged. The compaction force was set at 2000 N. Three types of tools were used to control prepreg tack: a steel table without any preparation, the same steel table sprayed with an epoxy glue and finally the same steel table covered by a first carbon-epoxy prepreg ply. The best results were obtained in the latter case, with a steering radius of 1.5 m without tow wrinkling (Fig. 10). It was not possible to quantify in-situ values of prepreg tack associated with these types of tools. However, we can state that the adhesion between prepreg plies was clearly higher than that between the prepreg ply and the metal, even when sprayed with glue. This confirms the strong influence of prepreg tack, shown in our study, in the occurrence of tow wrinkling.

### 5.3. Other experimental results

During validation tests, two other parameters, not taken into account in our model, were found to be very important in the

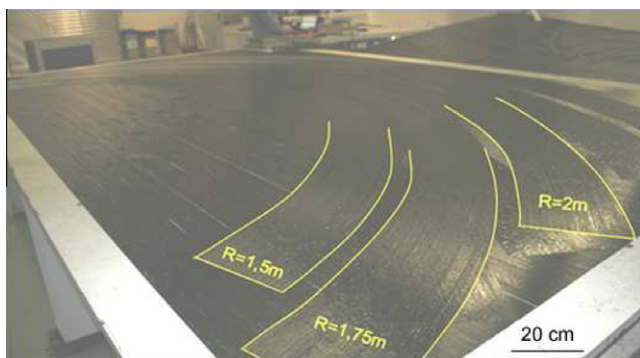


Fig. 10. Steered tow lay-down on a steel table covered by a first ply.

occurrence of tow wrinkling: the lay-down rate and the delay in tow wrinkling recovery. For productivity reasons, manufacturers are keen to use high lay-down rates. However, it was observed that high lay-down rates promote tow wrinkling occurrence. Typically, any other parameter being fixed, the minimum steering radius without tow wrinkling increases from 1.5 to 4 m when the lay-down rate increases from 12 to 30 m/min. Moreover, depending on processing parameters, tow wrinkling may recover many hours after fibre lay-down. These two observations suggest some sensitivity to time, temperature and frequency in the behaviour of the resin and the prepreg tack. The hypothesis of macro-homogeneity of the material used in this work does not enable these phenomena to be taken into account. A mesoscopic model, distinguishing the two constituents (carbon fibres and resin), should contribute to improving the estimation of tow wrinkling occurrence.

## 6. Conclusion

An analytical model was developed to estimate the critical buckling load of a tow and, consequently, the minimum steering radius for a circular fibre path. The Ritz method was used to derive closed-form solutions for the buckling loads. An original experiment, previously developed by our research group, was used to measure the normal foundation stiffness. Sensitivity analysis shows that the prepreg tack and the tow width strongly affect the critical load. It was found that the pure bending case gives the lowest values for the minimum steering radius. However, care must be taken to avoid stretching of the outer fibre of the tow to prevent lateral compressive stresses leading to a transverse buckling phenomenon. From a technological point of view, this study provides a domain in which the lay-up process does not encounter any buckling phenomenon. More precisely, it gives the minimum steering radius that does not induce tow wrinkling for a given normal stiffness and compaction force.

Further studies are foreseen by the authors to establish the relationship between the thermo-viscoelastic behaviour of the M21 resin and the normal stiffness  $k_N$ . If successful, this will allow thermal effects and lay-down rate to be incorporated into the model. Moreover, delay effects in tow wrinkling recovery may also be predicted.

## Acknowledgements

This work was supported by the FERMAT project of the French AESE (Aéronautique, Espace et Systèmes Embarqués) competitiveness cluster. The authors would like to thank Forest-Liné Capdenac, Hexcel Composite Dagneux and Airbus Nantes for their collaboration.

## References

- [1] Dominguez Fred S. Unidirectional tape prepreps. Eng Mater Handbook 1987;1:143–5 [composites].
- [2] Evans DO. Fiber placement in D.B. Miracle and S.L. Donaldson, ASM Handbook. ASM Int 2001;21:477–9 [composites].
- [3] Processing news. One-piece fuselage by fibre placement. Reinf Plast 2006;January:17.
- [4] Debout P, Chanal H, Duc E. Tool path smoothing of a redundant machine: application to automated fibre placement. Comput Aid Des 2011;43:122–32.
- [5] Lopes CS, Gurdal Z, Camanho PP. Variable-stiffness composite panels: buckling and first-ply failure improvements over straight-fibre laminates. Comput Struct 2008;86:897–907.
- [6] Blom AW, Setoodeh S, Hol Jan MAM, Gurdal Z. Design of variable-stiffness conical shells for maximum fundamental eigenfrequency. Comput Struct 2008;86:870–8.
- [7] Adam DOH, Hyer MW. Analysis of layer waviness in flat compression-loaded thermoplastic composite. J Eng Mater Technol - Trans ASME 1996;118(1):63–70.

- [8] Caiazzo A, Orlet M, McShane H, Strait L, Rachau C. The effects of marcel defects on composite structural properties. *Compos Struct: Theory Practice* 2001;1383:158–87.
- [9] Garnich MR, Karami G. Finite element micromechanics for stiffness and strength of wavy fiber composites. *J Compos Mater* 2004;38(4):273–92.
- [10] Adam DO, Hyer MW. The effect of layer waviness on the compression fatigue performance of thermoplastic composite laminates. *Int J Fatigue* 1994;16(6):385–91.
- [11] Adam DO, Hyer MW. The effect of layer waviness on the compression strength of thermoplastic composite laminates. *J Reinf Plast Compos* 1993;12(4):414–29.
- [12] Turoski Luke Everett. Effects of manufacturing defects on the strength of toughened carbon/epoxy prepreg composites. Master thesis, Montana State University, Bozeman, USA; 2000.
- [13] Nagendra S, Kodyialam S, Davis J, Parthasarathy V. Optimisation of tow fiber paths for composite design. In: *Proceeding of the AIAA/ASME/ASCE/AHS/ASC 36th structures, structural dynamics and materials conference*, New Orleans, LA, USA; 1995.
- [14] Ng SJ, Vizzini A. Mechanism of marcel formation in thick tapered composites. In: *Proceedings of the 34th international SAMPE technical conference*, Baltimore, MD, USA; 2002.
- [15] Zhou G. Preparation, structure and properties of advanced composites with long fibers and nanoparticles. PhD thesis. Ohio State University, USA; 2007.
- [16] Ahn KJ, Seferis JC, Pelton T, Wilhelm M. Analysis and characterization of prepreg tack. *Polym Compos* 1992;13:197–203.
- [17] Dubois O, Le Cam J-B, Beakou A. Experimental analysis of prepreg tack. *Exp Mech* 2010;50:599–606.
- [18] Ma X, Butterworth JW, Clifton C. Compressive buckling analysis of plates in unilateral contact. *Int J Solids Struct* 2007;44:2852–62.
- [19] Wright HD. Local stability of filled and encased steel section. *J Struct Eng – ASCE* 1995;121(17):1382–8.
- [20] Smith ST, Bradford MA, Oehlers DJ. Local buckling analysis of side-plated reinforced-concrete beam. I: Theoretical study. *J Struct Eng – ASCE* 1999;125(6):625–34.
- [21] Turvey GJ, Marshall IH, editors. *Buckling and postbuckling of composite plates*. London (UK): Chapman and Hall; 1995.
- [22] Timoshenko SP, Gere JM. *Theory of elastic stability*. New York (USA): McGraw-Hill; 1961.
- [23] Lekhnitskii SG. *Anisotropic plates*. New York (USA): Gordon and Breach; 1968.
- [24] Dickinson SM, Blasio AD. On the use of orthogonal polynomials in the Rayleigh–Ritz method for the study of the flexural vibration and buckling of isotropic and orthotropic rectangular plates. *J Sound Vib* 1986;108:51–62.
- [25] Gupta US, Ansari AH, Dharma S. Buckling and vibration of polar orthotropic circular plate resting on Winkler foundation. *J Sound Vib* 2009;297:457–76.
- [26] Robert NP. *Understanding structural mechanics*. Brunel Road, Salisbury (Wiltshire UK): Hi-Tech Scientific Ltd.
- [27] Beakou A, Mohamed A. Influence of variable scattering on the optimum winding angle of cylindrical laminated composites. *Compos Struct* 2001;53(3):287–93.
- [28] *Technical Fabrics Handbook*. HexForce reinforcements. US operations, Seguin, TX 78155, USA; March 2009. <<http://www.hexcel.com>>.
- [29] Lee HG, Hwang HY, Lee DG. Effect of wear debris on the tribological characteristics of carbon fiber epoxy composites. *Wear* 2006;261:453–9.
- [30] O'Brien DJ, Sottos NR, White SR. Cure-dependent viscoelastic Poisson's ratio of epoxy. *Exp Mech* 2007;47:237–49.
- [31] HexPly M21. Product data. US operations, Seguin, TX 78155, USA; March 2007. <<http://www.hexcel.com>>.
- [32] Lakrouf H, Sergot P, Creton C. Direct observation of cavitation and fibrillation in a probe tack experiment on model acrylic pressure-sensitive-adhesives. *J Adhes* 1999;69:307–59.
- [33] Friedl N, Rammerstorfer FG, Fischer FD. Buckling of stretched strips. *Comput Struct* 2000;78:185–90.